International Journal of Materials Chemistry and Physics
Vol. 1, No. 3, 2015, pp. 300-307
http://www.aiscience.org/journal/ijmcp

Growth and Properties Investigation of the $CuFe_{2.33}In_{9.67}S_{17.33}$ Single Crystal

S. V. Trukhanov[1, *], A. V. Trukhanov[1], I. V. Bodnar[2]

[1]Scientific Practical Materials Research Centre of NASB, Minsk, Belorussia
[2]Belarussian State University of Informatics and Radioelectronics, Minsk, Belorussia

Abstract

The $CuFe_{2.33}In_{9.67}S_{17.33}$ single crystals have been grown by the Bridgman method. The optical, magnetic and electrical properties investigations for this single crystal are carried out in 5-300 K temperature and 0-14 T magnetic field ranges. The variation of the spectral dependence of the absorption coefficient has been found. The band gap has been determined which is 1.5 eV. It is established that the sample studied is paramagnet. In ground state the ferromagnetic correlations of the short-range order typical for the spin glass with freezing temperature in range of 9 K are detected. The magnetic ordering temperature is almost 11 K. The sample studied is semiconductor with 15.2 kΩ*cm resistivity at room temperature. The magnetic and electrical states formation mechanism for the $CuFe_{2.33}In_{9.67}S_{17.33}$ single crystal is proposed.

Keywords

Magnetically Ordered Materials, Crystal Growth, Optical Properties, Exchange and Superexchange, Transmission Electron Microscopy, Magnetic Measurements

Received: August 31, 2015 / Accepted: September 13, 2015 / Published online: October 16, 2015

1. Introduction

Intensive development of nanoelectronics requires search and investigation of new efficient semiconductor materials. Magnetic semiconductors of $AB^{III}{}_2C^{VI}{}_4$ (A-Mn, Fe, Co, Ni; B^{III}-Ga, In; C^{VI}-S, Se, Te) type have an unusual combination of physical properties and are attractive due to the possibility of their use as a base element in nanoelectronics and in broadband phototransformator of optical radiation [1].

The ternary $FeIn_2S_4$ and $CuIn_5S_8$ compounds are such materials. These compounds crystallize in the cubic spinel structure and, as it has been shown by several authors, are promising materials for creation on their basis of devices for different purposes: Schottky diodes, switches, lasers, controlled by a magnetic field, light modulators, radiation-resistant solar energy converters, broadband photoconverters [2-4].

Spin-glass state is previously observed for the $FeIn_2S_4$ similar investigated compounds by other authors [5]. The semiconductors with spinel structure are good candidates for the spin glass behaviour [6] because the different types and degrees of disorder and frustration may be present in the lattice. The disorder may be due to a random magnetic dilution in one of the two sublattices, tetrahedral (A) and octahedral (B), and also to a random distribution of magnetic ions between the two sublattices. The frustration may be topological in type, as in the antiferromagnetic B-sublattice, like in $ZnCr_{2x}Ga_{2-2x}O_4$ [7], or due to the existence of competing of ferromagnetic and antiferromagnetic interactions, like in $ZnCr_{2x}In_{2-2x}S_4$ [8].

Previously, we investigated the magnetic, optical, electrical and thermal properties of the ternary compounds: $FeIn_2S_4$ [9], $MnIn_2S_4$ [10], $FeIn_2Se_4$ [11], as well as the solid solutions: $(In_2S_3)_x$ $(MnIn_2S_4)_{1-x}$, $(In_2S_3)_x$ $(FeIn_2S_4)_{1-x}$ [12], $(FeIn_2S_4)_x$ $(MnIn_2S_4)_{1-x}$ [13], $(FeIn_2S_4)_{1-x}$ $(CuIn_5S_8)_x$ [14, 15].

* Corresponding author
E-mail address: truhanov@ifttp.bas - net.by (S. V. Trukhanov)

This paper presents the results of a study of the optical, magnetic and electrical properties of the $CuFe_{2.33}In_{9.67}S_{17.33}$ single crystal.

2. Experimental Methods

The $CuFe_{2.33}In_{9.67}S_{17.33}$ single crystals were grown by the Bridgman method from the polycrystalline ingots obtained by the two-temperature method from the elementary components (copper, iron, indium and sulfur) with semiconductor purity by the technique described in [14].

These obtained ingots were crushed and reloaded in double quartz ampoules, the inner one is ended cylindrical capillaries. It ensures the formation of a single-crystal seed. The quartz rod was welded to the bottom of the outer ampoule, which serves as a holder. After evacuating the ampoule was placed in the one-band vertical furnace with a predetermined temperature gradient. In this furnace the growth of single crystals is performed. The furnace temperature was increased to 1400 K, and it was maintained at this temperature for 2 hs for homogenisation of the melt. After the exposure time the directional crystallization of the melt was carried out by decreasing the temperature of the furnace at a rate of ~ 2 K/h until complete solidification of the melt. For homogenisation the obtained ingots were annealed at 1020 K for 300 hs.

The elementwise composition of the grown $CuFe_{2.33}In_{9.67}S_{17.33}$ single crystals was determined by X-ray microprobe analysis on the "Cameca-SX100" installation at room temperature. The equilibrium of the obtained single crystals was determined by powder X-ray method. The angular positions of the lines of the diffraction spectra were recorded on a diffractometer DRON-3M in CuK_{α}-radiation with graphite monochromator at room temperature.

The transmission spectra in the fundamental absorption edge were recorded on a "Cary-500" spectrophotometer at room temperature. The plane-parallel plates perpendicular to the axis of the ingot were cut from the grown single crystals for optical measurements. Then these plates are mechanically ground and polished on both sides to a thickness of about 20 μm.

The investigation of the specific magnetic moment and electrical resistivity was performed using a universal cryogenic high-field measurement system-Liquid Helium Free High Field Measurement System (by Cryogenic Ltd, London, UK) in the temperature range 4-300 K and magnetic fields of 0-14 T [16]. The magnetic measurements were carried out on the single crystal samples, which were cut from obtained ingots with average size of 2 × 3 × 5 mm3. The measurements were realized as a temperature function in different fields of warming mode after cooling without field (ZFC) and with field (FC) [17]. The measurements of specific magnetic moment in the cooling field (FC) mode were carried out in the forward and backward direction of temperature change. The freezing temperature of the magnetic moments of ferromagnetic clusters (T_f) was determined as the temperature corresponding to the maximum of ZFC-curve. The temperatures of initial divergence ZFC-and FC-curves with the increasing (T_{rev}) and decreasing (T_x) temperatures were determined in the points where the differences exceed 3%. The temperature of magnetic ordering (T_{mo}) was determined from the temperature dependence of the FC-curve such as equivalent point to the minimum of the FC-curve temperature derivative ($\min\{dM_{FC}/dT\}$). The magnetic ordering temperature is a well-defined quantity which characterizes, in addition, beginning a wide temperature range of transition of the substance under consideration in the paramagnetic state [18]. In the minimum point of the derivative the behavior nature with temperature of the FC-curve varies from the "curved up" to the "curved down", which corresponds to its transition from rapid decay to slow. Thus, the magnetic ordering temperature determines the end of the rapid decay of the magnetic moment with the temperature increase [19]. The spontaneous atomic magnetic moment (σ_s) was determined from the field dependence of the linear extrapolation to zero field.

The dependence of the electrical resistivity was measured by a standard four-probe method [20]. The contacts were formed using ultrasonic soldering by indium solder. For measurements the high quality samples were used in the shape of parallelepiped with average dimensions of 8 × 4 × 4 mm^3. The direction of electric current coincides with the long side of the sample. The magnetic field was applied parallel to the electric current in the sample. The activation energy was calculated using the equation: $E_{ac} = 2k_B*\{\partial (\ln\rho) / \partial (T^{-1})\}$, where E_{ac}-activation energy, k_B-Boltzmann's constant ($8.617*10^{-5}$eV*K^{-1}), ρ-resistivity. Magnetoresistance was calculated according to the formula: MR (%) ={ [ρ (H)-ρ (0)] /ρ (0)}*100 %, where MR (%)-negative isotropic magnetoresistance, expressed as a percentage, ρ (H) – resistivity in a magnetic field, ρ (0) – the electrical resistivity in zero magnetic field. The analysis of the experimental data and numerical calculations were performed using the computer program Origin 7.5 [21].

3. Results and Discussion

The results of X-ray microprobe analysis showed that the content of elements in the single crystals grown (Cu: Fe: In: S = 3.19: 7.55: 31.84: 57.42 at. %) is in good agreement

with the predetermined composition in the starting batch (Cu: Fe: In: S = 3.30 7.68: 31.88; 57.14 at.%) and no significant variations in the composition at the various points of the single crystals. This indicates on their homogeneity.

The powder XRD pattern for the $CuFe_{2.33}In_{9.67}S_{17.33}$ single crystal is shown in Fig. 1. The reflection angles, interplanar distances, intensities of the diffraction maxima and Miller indices are presented in the table 1. It is evident that on the available diffraction pattern the reflections indices characteristic for the cubic spinel structure are presented (Fig. 1, Table 1). Good resolution of the high-angle lines indicates the equilibrium of the grown single crystals. The unit cell parameter calculated by the method of least squares is a = 10.635 ± 0.005 Å.

Table 1. Radiometric data of $CuFe_{2.33}In_{9.67}S_{17.33}$ single crystal.

2θexp	2θtheor	dexp	dtheor	hkl	I
14.41	14.41	6.14	6.14	111	9
23.65	23.64	3.76	3.76	220	29
27.81	27.80	3.207	3.206	311	100
29.06	29.06	3.0701	3.0701	222	8
33.68	33.68	2.6588	2.6588	400	27
41.56	41.56	2.1709	2.1709	422	13
44.23	44.21	2.0467	2.0467	511	36
48.38	48.37	1.8797	1.8801	440	65
50.75	50.74	1.7976	1.7977	531	39
54.55	54.52	1.6808	1.6817	620	59
56.74	56.71	1.6212	1.6218	533	11
57.44	57.43	1.6029	1.6031	622	5
60.26	60.24	1.5347	1.5350	444	5
65.65	65.64	1.4209	1.4211	642	5
67.63	67.60	1.3841	1.3845	731	21
70.82	70.82	1.3293	1.3293	800	7
75.84	75.84	1.2533	1.2533	822	3
77.70	77.69	1.2279	1.2280	751	12
80.76	80.75	1.1889	1.1890	840	4
87.42	87.40	1.1147	1.1149	931	9

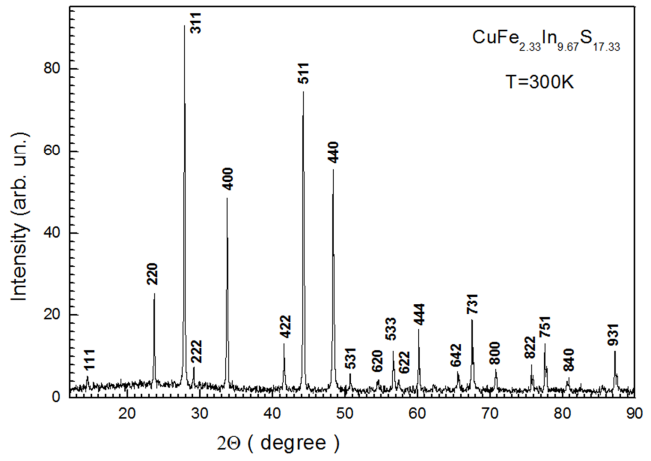

Fig. 1. Powder X-ray diffraction partten for the $CuFe_{2.33}In_{9.67}S_{17.33}$ single crystal.

The transmission spectrum of the single crystal is shown in Fig. 2. It can be seen that the spectrum has shown the complex behavior nature in the investigated wavelengths range. The range consists of three sections: the first section begins to grow the value of the transmission, then there is a slowdown in the transmission, followed by a further increase in the value of the transmission.

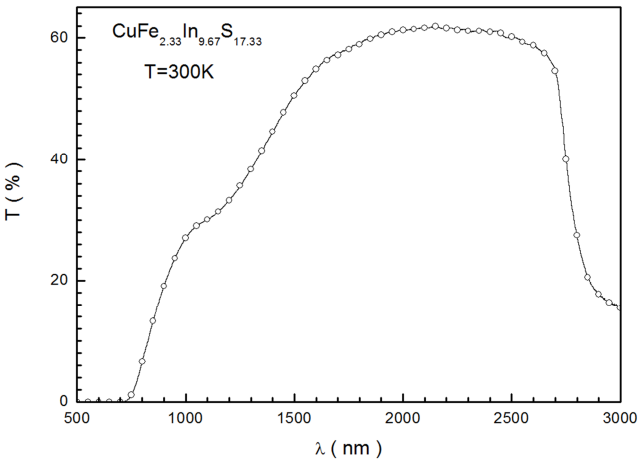

Fig. 2. The transmission spectrum at room temperature for the $CuFe_{2.33}In_{9.67}S_{17.33}$ single crystal.

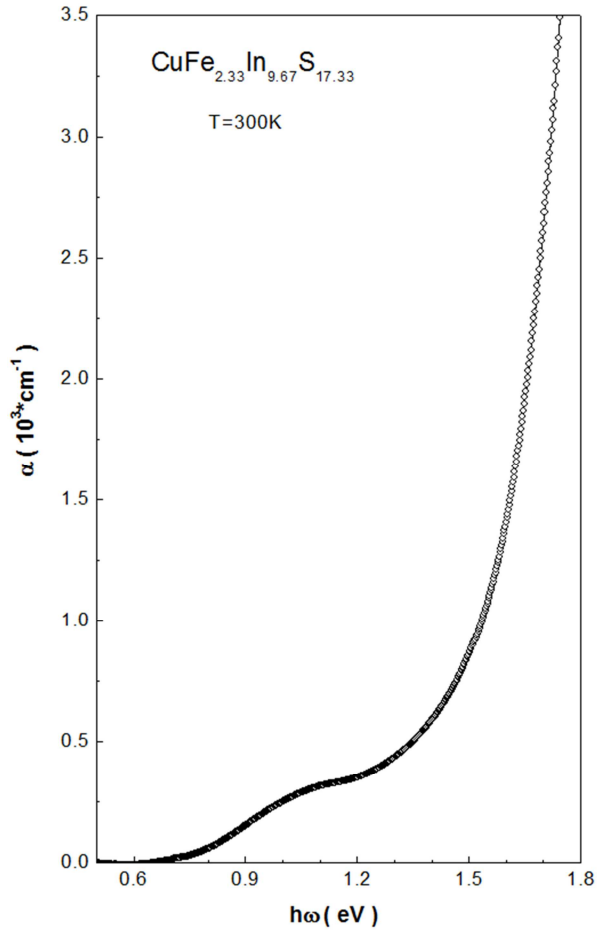

Fig. 3. The spectral dependence of the α absorption coefficient versus the ħω photon energy for the $CuFe_{2.33}In_{9.67}S_{17.33}$ single crystal.

As a registered transmission spectra the absorption coefficient was calculated according to the formula that takes into account multiple internal reflection in a plane-parallel sample:

$$\alpha = \frac{1}{d}\ln\left\{\frac{(1-R)^2}{2T} + \sqrt{\left[\frac{(1-R)^2}{2T}\right]^2 + R^2}\right\} \quad (1)$$

Where in α-absorption coefficient, d-sample thickness, R-reflectance.

Fig. 3 shows the spectral dependence of the α absorption coefficient versus the ħω photon energy for the $CuFe_{2.33}In_{9.67}S_{17.33}$ single crystal calculated in accordance with expression (1). It is evident that all these single crystals have a large quantity of absorption ($\alpha > 10^3$ cm^{-1}). In the energy range of 0.70-1.05 eV the absorption coefficient increases, then its growth somewhat slows down and at the energy > 1.3 eV it begins a sharp increase of the absorption coefficient versus ħω.

Due to the lack of theoretical calculations of the band structure of like $AB^{III}{}_2C^{VI}{}_4$ compounds the interpretation of the observed bands in the fundamental absorption edge of the $CuFe_{2.33}In_{9.67}S_{17.33}$ single crystal is difficult performed task. However, we can assume (by analogy with $FeIn_2S_4$ [22]) that the increase in α with ħω increase in the 0.70-1.05 eV energy range associated with the start of interband transitions in the investigated single crystal. The sharp increase of α in the 1.3-1.8 eV energies indicates that the absorption edge is due to the direct interband transitions.

Fig. 4 shows the $(\alpha\cdot\hbar\omega)^2$ spectral dependence versus ħω photon energy. Bandgap is determined by extrapolating of the straight sections of $(\alpha\cdot\hbar\omega)^2$ dependence to the intersection with the horizontal axis. The value of E_g for the $CuFe_{2.33}In_{9.67}S_{17.33}$ single crystal is 1.532 ± 0.005 eV.

As it is known [9], the $FeIn_2S_4$ compound is characterized the magnetic ordering temperature $T_{mo} \approx 22$ K. The T_{mo} magnetic ordering temperature is shifted to higher temperatures with increasing field. The absence of differences in the measurement of FC-curves in both forward and reverse temperature changes is established, which is observed in classical second-order magnetic transitions [23]. In the vicinity of 12 K, the decrease of the specific magnetic moment with temperature decreasing is seen. Such behavior may be characteristic of the antiferromagnetic state [24].

It was found at the measuring of the specific magnetic moment of $CuFe_{2.33}In_{9.67}S_{17.33}$ single crystal that it is paramagnetic (Fig. 5). Specific magnetic moment increases monotonically with decreasing temperature. Below 10 K, there is a tendency to saturate of the specific magnetic moment. The magnetic ordering temperature is about 11 K. The increase in the magnetic field from 1 T to 5 T naturally increases the specific magnetic moment and magnetic ordering temperature [25].

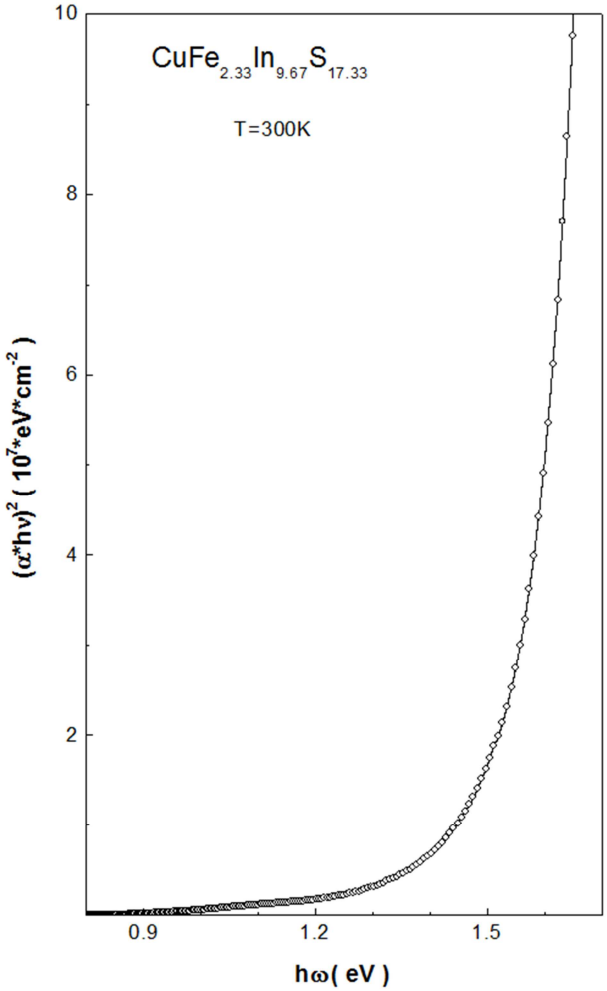

Fig. 4. The spectral dependence of the $(\alpha\cdot\hbar\omega)^2$ versus the ħω photon energy for the $CuFe_{2.33}In_{9.67}S_{17.33}$ single crystal.

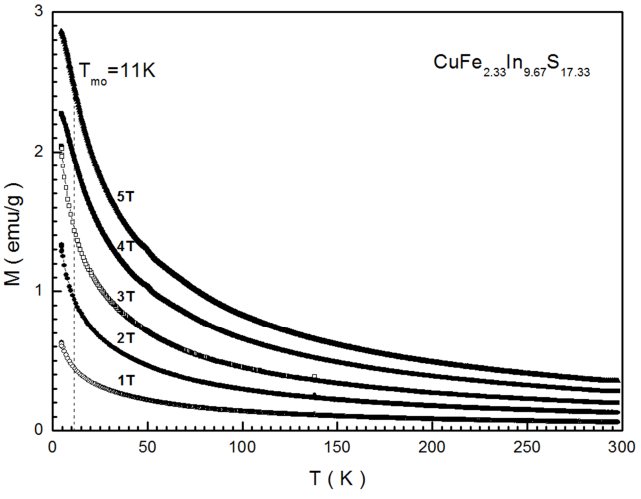

Fig. 5. Temperature dependence of the specific magnetic moment in fields of 1 T (open circles), 2 T (full circles), 3 T (open boxes), 4 T (full boxes) and 5 T (full triangles) for the $CuFe_{2.33}In_{9.67}S_{17.33}$ single crystal.

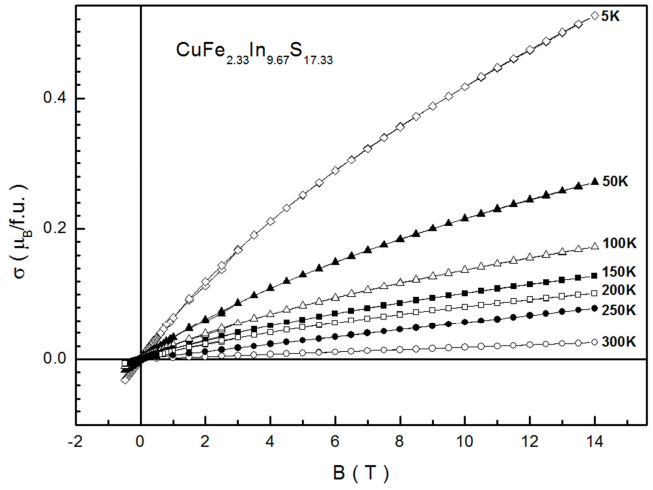

Fig. 6. Field dependence of the atomic magnetic moment at temperatures 5 K (open diamonds), 50 K (full triangles), 100 K (open triangles), 150 K (full boxes), 200 K (open boxes), 250 K (full boxes) and 300 K (open circles) for the $CuFe_{2.33}In_{9.67}S_{17.33}$ single crystal.

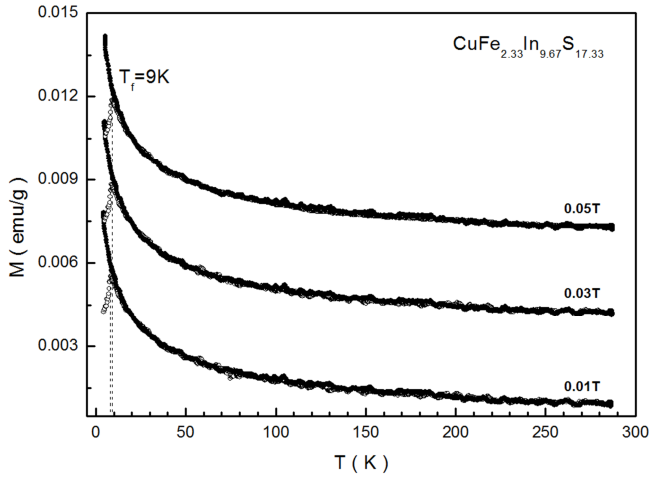

Fig. 7. Temperature dependence of ZFC (open circles) and FC curves (full circles) of the specific magnetic moment in fields of 0.01 T, 0.03 T and 0.05 T for the $CuFe_{2.33}In_{9.67}S_{17.33}$ single crystal.

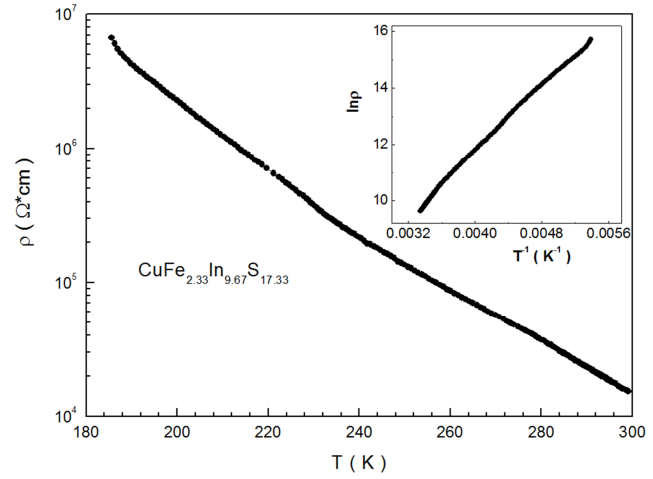

Fig. 8. Temperature dependence of the electrical resistivity in zero field for the $CuFe_{2.33}In_{9.67}S_{17.33}$ single crystal. Inserts demonstrates dependence of resistivity logarithm versus inverse temperature.

It has seen from the field dependences of the σ atomic magnetic moment (Fig. 6) that they are almost linear even at the lowest temperatures. This is characteristic of antiferromagnetic or paramagnetic state. In a magnetic field of 14 T the value of the atomic magnetic moment is 0.03 μ_B/f.u. at a temperature of 300 K, increasing up to 0.53 μ_B/f.u. at a temperature of 5 K. The divalent iron cations have 4 unpaired d-electrons. Insignificant value of the atomic magnetic moment indicates likely the partial antiferromagnetic ordering of the Fe^{2+} cations. The non-zero values of the spontaneous and residual atomic magnetic moment and the coercive force are observed at low temperatures (~ 5 K), which is peculiar to ferromagnetic ordered state or the presence of ferromagnetic correlations of the short-range order [26]. This behavior does not correspond to the homogeneous antiferromagnetic state.

The results of measurements of the ZFC and FC dependences of the magnetic moment in weak fields are shown in Fig. 7. It was found that at low temperatures (<12 K) the ZFC curves decrease with decreasing temperature faster than the FC curves. In this case the ZFC curves decrease more sharply. On the ZFC curve the peak is observed. It is characteristic of the magnetic phase state of a spin glass [27]. T_f freezing temperature increases slightly with field increase.

Fig. 8 shows the temperature dependence of the electrical resistivity. It continuously increases with decreasing temperature and demonstrates the activation behavior. Any anomalies in the resistivity dependence were not observed over the entire temperature range. At room temperature (300 K) the investigated sample has a resistivity value equal to the 15.2 kΩ*cm. An increase in resistivity by almost 3 orders of magnitude was detected with decreasing temperature. Magnetoresistance correlates with the absence of any anomalies in the electrical resistivity at the transition to magnetically ordered state, and gradually increased reaching of its maximum value < 1 % in a field of 5 T at low temperature. At room temperature magnetoresistance is absent. This behavior is due to the tunneling magnetoresistance of the nature of the charge transport [28].

It should be noted that the resistivity is satisfactorily described by the $\ln\rho \sim T^{-1}$ equation. Two linear sections with different angles at high and low temperatures are released on the $\ln\rho \sim T^{-1}$ dependences (inset in Fig. 8). The low-temperature region corresponds to the impurity conductivity, while the high-temperature region-their own. The activation energy is determined on the angle of inclination of the tangent, which at room temperature is ~ 0.3 eV.

Magnetic semiconductors are characterized by the presence of so-called indirect exchange interaction between the d-ions. In the crystal lattice of the magnetic semiconductor d-cations

are separated by nonmagnetic cations, and therefore the wave functions of d-electrons do not directly overlap. Direct exchange interaction between them is missing. However, there is an indirect interaction due to the fact that the wave functions of d-cations overlap of the wave functions of nonmagnetic cations. Typically, for the degenerate magnetic semiconductors distinguish indirect magnetic 180-or 90-degree exchange interactions, which can be, depending on the implementation of conditions, so as ferromagnetic or antiferromagnetic.

According to the empirical Goodenough-Kanamori rules [29-31] for the cations in octahedral anion coordination the 180-degree indirect exchange interactions between the magnetic moments of the electrons at the partially filled and fully unoccupied energy levels are negative. Therefore, the indirect exchange interactions between Fe^{2+}-S^{2-}- Fe^{2+} with different coordination of the Fe^{2+} cations must be predominantly antiferromagnetic. The antiferromagnetic state in the $FeIn_2S_4$ like compounds was found earlier [9], as well as by other authors [32, 33]. If there is some structural anomaly the breakage of long-range Fe^{2+}-S^{2-}- Fe^{2+} exchange chains may occur. This is so-called diamagnetic dilution, which can lead to the formation of an inhomogeneous magnetic state. The indirect 180-degree exchange interactions between the magnetic moments of electrons at the fully and partially filled energy levels and completely filled energy levels are positive.

Thus the ferromagnetic short-range nanoscale ordering correlations may appear in dilute magnetic subsystem [15]. Competition between nanoscale antiferromagnetic and ferromagnetic interactions of iron cations leads to the frustration of exchange bonding and the formation of new magnetic phase-the spin glass state. The exchange bonding is called frustrated provided that the relative orientation of the magnetic moments does not coincide with the sign of their exchange interactions. The spin glass state is previously observed for the $FeIn_2S_4$ like compounds by other authors [34, 35].

The neutron diffraction and AC low field susceptibility measurements at different frequencies have been realized in work [5] for the $FeIn_2S_4$ compound. The neutron diffraction patterns do not exhibit any additional Bragg lines at 1.5 K to patterns at 300 K. The modulation of the neutron diffraction patterns background has been interpreted on the Burlet model [36] for spin-spin correlations and the different scattering intensities have been analysed. It is necessary to use 8 parameters in contrary of $FeGa_2O_4$ for describing of the spin-spin correlations in $FeIn_2S_4$ that means that the compound is not very close to establish an ordered magnetic state. In this case the magnetic state may be described by the nanoscale $r_{nc} > 50$ nm ferromacnetic clusters which are invisible for the diffraction. A different behaviour is observed for the FC susceptibility, which increases with temperature decreasing for $FeGa_2O_4$, almost remains constant for $FeAl_2O_4$ and decreases after a maximum for $FeIn_2S_4$. These differences should reflect the different extent of magnetic correlations in the three spinels. Therefore, the strong spin glass character is observed for the sulfide compound while less pronounced one for the oxide compounds.

In work [35] it has been shown that the high-temperature susceptibility fits to the $MnIn_2S_4$ and indicates the existence of antiferromagnetic exchange interactions. The low-field magnetization data shown a peak at 5.6 K, below which strong irreversibility is observed between ZFC and FC cycles suggesting that the observed peak corresponds to a nanoscale spin glass like transition instead of the antiferromagnetic one previously reported [37]. Further evidence of this magnetic state comes from AC susceptibility data at different frequencies. The in-phase component χ (T) of AC susceptibility exhibits the behaviour expected of spin glasses, i.e. a shift of the cusp to higher temperatures for higher frequencies. The large deviation from the Curie–Weiss behavior was due to strong dominant antiferromagnetic interactions between Mn ions [38]. It is interesting to note that the θ paramagnetic Curie value is more than one order of magnitude larger than T_f, i.e., $\theta/T_f \approx 25$. This high θ/T_f value is consistent with the existence of nanoscale magnetic frustration expected for a spin-glass system.

The spin glass properties are not completely understood. Comprehension of the magnetic spin glass state nature is important for the development of fundamental physics. This comprehension may lead to new applications of spin glasses. The analogy between a set of nearly degenerate low-lying metastable states of cooled spin glasses and function of human memory has been previously established. Therefore, it is possible that the study of spin glasses will help to create principles of computer memory [39].

The nanocluster spin glass state is often observed in heterogeneous magnetic systems, such as alloys of Co-Cu and Co-Ag [40]. The ferromagnetic nanoclusters are embedded in non-ferromagnetic (paramagnetic or antiferromagnetic) matrix. The quantitative estimate of the average size of ferromagnetic clusters can be performed. For this purpose it is necessary to use the Bean-Livingstone formula [41], which relates to the average size of ferromagnetic clusters and magnetic crystallografic anisotropy constant, which presents the volume energy density of the magnetic crystallografic anisotropy, and critical temperature T_f:

$$\langle K\rangle\langle V\rangle = k_B T_f$$

where $\langle K\rangle$-the average value of the magnetic crystallografic

anisotropy constant of the ferromagnetic cluster, ⟨V⟩-its average volume, k_B-Boltzmann constant, T_f-temperature of freezing (for a maximum of ZFC-curve). Anisotropy constant can be obtained from the equation for the energy magnetic crystallografic anisotropy in the (100) plane:

$$E_a = K_1 \sin^2(\theta) + K_2 \sin^4(\theta)$$

where K_1, K_2-constants of magnetic crystallografic anisotropy, θ-the angle between the magnetization and the [010] axis. The energy of the magnetic crystallografic anisotropy is determined by the area between the curves M (B) measured for single crystals along the [010] and [001] directions. So the average size of ferromagnetic inclusions is about 10 nm for the anion-deficient manganite $La_{0.70}Sr_{0.30}MnO_{2.85}$ with $T_f \sim 40$ K [26]. The T_{rev} temperature of ZFC and FC-curves divergence was measured in the same mode of temperature change and it determines the maximum size of the ferromagnetic cluster [42], which almost coincides with the average size in this case. The decrease of the freezing T_f temperature indicates a decreasing of the average size of the ferromagnetically ordered clusters [43].

4. Conclusions

Thus, in the present study the optical, magnetic and electrical properties of the $CuFe_{2.33}In_{9.67}S_{17.33}$ single crystal are investigated. The variation of the spectral dependence of the absorption coefficient is found. The band gap is determined, which is 1.5 eV. It is established that the investigated sample is paramagnetic. It is found that the some of the indirect exchange interactions in the ground state between the Fe^{2+} cations has antiferromagnetic character along with ferromagnetic correlations of short-range order. The main magnetic phase state of the studied compounds is a spin glass one with freezing temperature in vicinity of 9 K. The magnetic ordering temperature is about 11 K. The investigated sample is a semiconductor with a 15.2 kΩ*cm resistivity at room temperature. The most probable cause and mechanism of formation of magnetic and electric states for the $CuFe_{2.33}In_{9.67}S_{17.33}$ single crystal are discussed.

References

[1] G. Dagan, S. Endo, G. Hodes, G. Zawatzky, D. Gahen, Sol. Energy Mater. 11 (1984) 57.

[2] H. Lewerenz, H. Kozlowsky, K.D. Husemann, Nature 321 (1986) 687.

[3] A.V. Vedyaev, Phys. Usp. 45 (2002) 1296.

[4] T. Torres, V. Sagredo, L.M. de Chalbaud, G. Attolini, F. Bolzoni, Physica B 384 (2006) 100.

[5] J.L. Soubeyroux, D. Fiorani, E. Agostinelli, S.C. Bhargava, J.L. Dormann, Journal De Physique 49 (1988) 1117.

[6] J. Villain, Z. Phys. B 33 (1979) 31.

[7] D. Fiorani, S. Viticoli, J. L. Dorman, J. L. Tholence, A.P. Murani, Phys. Rev. B 30 (1984) 2776.

[8] M. Alba, J. Hamman, M. Nogues, J. Phys. C 15 (1982) 5441.

[9] I.V. Bodnar, S.V. Trukhanov, Semiconductors 45 (2011) 861.

[10] I.V. Bodnar, S.V. Trukhanov, S.A. Pauliukavets, M.A. Novikova, J. Spintronics and Magnetic Nanomater. 1 (2012) 75.

[11] I.V. Bodnar, S.A. Pavlyukovets, S.V. Trukhanov, Yu.A. Fedotova, Semiconductors 46 (2012) 606.

[12] I.V. Bodnar, M.A. Novikova, S.V. Trukhanov, Semiconductors 47 (2013) 596.

[13] I.V. Bodnar, S.V. Trukhanov, Semiconductors 45 (2011) 1408.

[14] I.V. Bodnar, S.V. Trukhanov, Semiconductors 48 (2014) 705.

[15] S.V. Trukhanov, I.V. Bodnar, M.A. Zhafar, J. Magn. Magn. Mater. 379 (2015) 22.

[16] S.V. Trukhanov, A.V. Trukhanov, A.N. Vasiliev, H. Szymczak, JETP 111 (2010) 209.

[17] S.V. Trukhanov, A.V. Trukhanov, H. Szymczak, Low Temp. Phys. 37 (2011) 465.

[18] S.V. Trukhanov, Physics of the Solid State 53 (2011) 1845.

[19] S.V. Trukhanov, A.V. Trukhanov, A.N. Vasil'ev, A. Maignan, H. Szymczak, JETP Letters 85 (2007) 507.

[20] S. V. Trukhanov, A. V. Trukhanov, H. Szymczak, C. E. Botez, A. Adair, J. Low Temp. Phys. 149 (2007) 185.

[21] S. V. Trukhanov, J. Mater. Chem. 13 (2003) 347.

[22] I. V. Bodnar, S. A. Pavlukovets, Semiconductors 45 (2011) 1395.

[23] S. V. Trukhanov, JETP 100 (2005) 95.

[24] V. D. Doroshev, V. A. Borodin, V. I. Kamenev, A. S. Mazur, T. N. Tarasenko, A. I. Tovstolytkin, S. V. Trukhanov, J. Appl. Phys. 104 (2008) 093909.

[25] S. V. Trukhanov, A. V. Trukhanov, A. N. Vasiliev, A. M. Balagurov, H. Szymczak, JETP 113 (2011) 820.

[26] S. V. Trukhanov, JETP 101 (2005) 513.

[27] S. V. Trukhanov, A. V. Trukhanov, S. G. Stepin, H. Szymczak, C. E. Botez, Physics of the Solid State 50 (2008) 886.

[28] S. V. Trukhanov, A. V. Trukhanov, C. E. Botez, A. H. Adair, H. Szymczak, R. Szymczak, J. Phys.: Condens. Matter. 19 (2007) 266214.

[29] J. B. Goodenough, Phys. Rev. 100 (1955) 564.

[30] J. Kanamori, J. Phys. Chem. Sol. 10 (1959) 87.

[31] J. B. Goodenough, A. Wold, R. J. Arnott, N. Menyuk, Phys. Rev. 124 (1961) 373.

[32] T. Kanomata, H. Ido, T. Kaneko, J. Phys. Soc. Jpn. 34 (1973) 554.

[33] B. S. Son, S. J. Kim, C. S. Kim, M. H. Jung, Y. Jo, J. Korean Phys. Soc. 52 (2008) 1077.

[34] J. L. Dormann, M. Seqqat, D. Fiorani, M. Nogues, J. L. Soubeyroux, S. C. Bhargava, P. Renaudin, Hyperfine Interactions 54 (1990) 503.

[35] V. Sagredo, M. C. Mororón, L. Betancourt, G. E. Delgado, J. Magn. Magn. Mater. 312 (2007) 294.

[36] P. Burlet, E. F. Bertaut, Solid State Commun. 5 (1967) 279.

[37] C. I. Hsu, J. J. Steger, E. A. Demeo, A. Wold, G. S. Heller, J. Solid State Chem. 13 (1975) 304.

[38] G. Goya, V. Sagredo, Phys. Rev. B 64 (2001) 235208.

[39] M. H. Kruder, A. B. Bortz, Phys. Today 37 (1984) 20.

[40] S. Nafis, J. A. Woollam, Z. S. Shan, D. J. Sellmyer, J. Appl. Phys. 70 (1991) 6050.

[41] C. P. Bean, J. D. Livingstone, J. Appl. Phys. 30 (1959) S120.

[42] S. V. Trukhanov, A. V. Trukhanov, H. Szymczak, J. Phys. Chem. Sol. 67 (2006) 675.

[43] S.V. Trukhanov, V.V. Fedotova, A.V. Trukhanov, H. Szymczak, C. E. Botez, Technical Physics 53 (2008) 49.